EINDHOVEN UNIVERSITY OF TECHNOLOGY

# Plasma-enhanced and thermal atomic layer deposition of Al2O3 using dimethylaluminum isopropoxide , [Al(CH3)2(μ-OiPr)]2, as an alternative aluminum precursor

*Citation for published version (APA):*
Potts, S. E., Dingemans, G., Lachaud, C., & Kessels, W. M. M. (2012). Plasma-enhanced and thermal atomic layer deposition of Al2O3 using dimethylaluminum isopropoxide , [Al(CH3)2(μ-OiPr)]2, as an alternative aluminum precursor. *Journal of Vacuum Science and Technology A: Vacuum, Surfaces, and Films*, *30*(2), 021505-1/15. [021505]. https://doi.org/10.1116/1.3683057

*DOI:*
10.1116/1.3683057

*Document status and date:*
Published: 01/01/2012

*Document Version:*
Publisher's PDF, also known as Version of Record (includes final page, issue and volume numbers)

*Please check the document version of this publication:*

• A submitted manuscript is the version of the article upon submission and before peer-review. There can be important differences between the submitted version and the official published version of record. People interested in the research are advised to contact the author for the final version of the publication, or visit the DOI to the publisher's website.
• The final author version and the galley proof are versions of the publication after peer review.
• The final published version features the final layout of the paper including the volume, issue and page numbers.

Link to publication

*General rights*
Copyright and moral rights for the publications made accessible in the public portal are retained by the authors and/or other copyright owners and it is a condition of accessing publications that users recognise and abide by the legal requirements associated with these rights.

• Users may download and print one copy of any publication from the public portal for the purpose of private study or research.
• You may not further distribute the material or use it for any profit-making activity or commercial gain
• You may freely distribute the URL identifying the publication in the public portal.

If the publication is distributed under the terms of Article 25fa of the Dutch Copyright Act, indicated by the "Taverne" license above, please follow below link for the End User Agreement:

www.tue.nl/taverne

*Take down policy*
If you believe that this document breaches copyright please contact us at:

openaccess@tue.nl

providing details and we will investigate your claim.

Download date: 23. Aug. 2022

# Plasma-enhanced and thermal atomic layer deposition of $Al_2O_3$ using dimethylaluminum isopropoxide, $[Al(CH_3)_2(\mu\text{-}O^iPr)]_2$, as an alternative aluminum precursor

Stephen E. Potts[a] and Gijs Dingemans
*Department of Applied Physics, Eindhoven University of Technology, P. O. Box 513, 5600 MB Eindhoven, The Netherlands*

Christophe Lachaud
*Air Liquide Research & Development, 1 Chemin de la Porte des Loges, BP 126, 78345 Jouy-en-Josas, France*

W. M. M. Kessels[b]
*Department of Applied Physics, Eindhoven University of Technology, P. O. Box 513, 5600 MB Eindhoven, The Netherlands*

(Received 10 November 2011; accepted 19 January 2012; published 17 February 2012)

The authors have been investigating the use of $[Al(CH_3)_2(\mu\text{-}O^iPr)]_2$ (DMAI) as an alternative Al precursor to $[Al(CH_3)_3]$ (TMA) for remote plasma-enhanced and thermal ALD over wide temperature ranges of 25–400 and 100–400 °C, respectively. The growth per cycle (GPC) obtained using *in situ* spectroscopic ellipsometry for plasma-enhanced ALD was 0.7–0.9 Å/cycle, generally lower than the >0.9 Å/cycle afforded by TMA. In contrast, the thermal process gave a higher GPC than TMA above 250 °C, but below this temperature, the GPC decreased rapidly with decreasing temperature. Quadrupole mass spectrometry data confirmed that both $CH_4$ and $HO^iPr$ were formed during the DMAI dose for both the plasma-enhanced and thermal processes. $CH_4$ and $HO^iPr$ were also formed during the $H_2O$ dose but combustion-like products ($CO_2$ and $H_2O$) were observed during the $O_2$ plasma dose. Rutherford backscattering spectrometry showed that, for temperatures >100 °C and >200 °C for plasma-enhanced and thermal ALD, respectively, films from DMAI had an O/Al ratio of 1.5–1.6, a H content of ∼5 at. % and mass densities of 2.7–3.0 g $cm^{-3}$. The film compositions afforded from DMAI were comparable to those from TMA at deposition temperatures ≥150 °C. At lower temperatures, there were differences in O, H, and C incorporation. 30 nm thick $Al_2O_3$ films from the plasma-enhanced ALD of DMAI were found to passivate *n*- and *p*-type Si floatzone wafers (∼3.5 and ∼2 Ω cm, respectively) with effective carrier lifetimes comparable to those obtained using TMA. Surface recombination velocities of < 3 and < 6 cm $s^{-1}$ were obtained for the *n*- and *p*-type Si, respectively. Using these results, the film properties obtained using DMAI and TMA are compared and the mechanisms for the plasma-enhanced and thermal ALD using DMAI are discussed. © *2012 American Vacuum Society*. [DOI: 10.1116/1.3683057]

## I. INTRODUCTION

Ultra-thin $Al_2O_3$ films deposited using atomic layer deposition (ALD) have many prominent applications, not only as medium-*k* dielectrics,[1–3] but also as passivation layers in solar cells,[4–9] moisture barriers for organic electronics[10–12] and anti-corrosion coatings for metallic substrates.[13–15] For several of these applications, ALD at relatively low deposition temperatures is preferred or, in some cases, required. Therefore, plasma-enhanced ALD could be implemented as a technique for depositions at temperatures as low as room temperature.[16,17] $[Al(CH_3)_3]$ (TMA) is a popular Al precursor as it exhibits almost ideal ALD growth characteristics, even down to room temperature. However, its main drawback is its highly pyrophoric nature.

The search for safer precursors for use in industrial-scale high-volume manufacturing is ongoing (see Sec. II for more information on Al precursors). The use of $[Al(CH_3)_2(\mu\text{-}O^iPr)]_2$ (DMAI, $^iPr$ = isopropyl) as an alternative Al precursor to TMA has been investigated, both for low pressure CVD[18] and ALD with $H_2O$[19] and a direct $O_2$ plasma.[20] For ALD with $H_2O$,[19] no clear ALD window was observed, whereas it was claimed a wider ALD window was obtained using DMAI for direct plasma ALD.[20] In order to better understand the underlying mechanism of ALD using DMAI and TMA, remote plasma-enhanced and thermal ALD were investigated in the same reactor over wide temperature ranges of 25–400 and 100–400 °C, respectively. The characteristics of the DMAI ALD process are compared with those of TMA in the same reactor, which were reported previously.[17] The application of $Al_2O_3$ films as surface passivation layers for *n*- and *p*-type floatzone Si wafers using DMAI as a precursor is also addressed.

## II. PRECURSOR CONSIDERATIONS AND PROPERTIES

By far the most popular precursor for Al-containing films is the aforementioned TMA. It has been employed in a variety of chemical vapor deposition (CVD) processes to $Al_2O_3$,[21–24] AlN,[25,26] and Al metal;[27] and it is also ubiquitous in the ALD

[a]Electronic mail: s.e.potts@tue.nl
[b]Electronic mail: w.m.m.kessels@tue.nl

of $Al_2O_3$ using water,[28–34] hydrogen peroxide,[35] alcohols,[36] ozone,[37–42] or an $O_2$ plasma[12,43–47] as the oxygen source. However, despite its high vapor pressure and excellent ALD characteristics, alternatives to TMA are being sought. The two main reasons for this are its high reactivity with water (such that powder-based fire-control systems are implemented as opposed to water-based) and its highly pyrophoric nature. For TMA specifically, this pyrophoricity most likely arises from (a) the lower mean bond energy of Al–C bonds compared with Al–X (X = N, O, halide)[48] and (b) the insufficient filling of the vacant $p_z$ orbital on the Al center, leaving the molecule (more) vulnerable to nucleophilic attack.

As with all trivalent Al compounds, the TMA molecule partially compensates for the latter by forming a dimer. This occurs as a method by which the Al center can obtain electronic saturation (i.e., a full octet), generally via dative bonding of a ligand on one Al center to the vacant $p_z$ orbital on another. For TMA, the dimerization mechanism differs from this, whereby the Al atoms are bridged by methyl groups forming a three-center-two-electron bond.[49–52] However, in the gas phase the dimer is in equilibrium with the monomer, with the monomer prevailing at higher temperatures;[53,54] for example, at a pressure of 30 Torr, 3% of the TMA monomer is present at 60 °C, compared with 96% at 215 °C.[54] Therefore, dimerization does not significantly reduce the pyrophoricity of TMA.

Because of the hazards presented by the pyrophoricity of TMA, alternative Al precursors have been investigated. Addition of Lewis-basic ligands, such as halides, OR or $NR_2$, or donor-functionalized ligands, such as 1-methoxy-2-methyl-2-propoxide (mmp), offer the coordinative saturation required to reduce/eliminate pyrophoricity. Perhaps the most favored alternatives to TMA are halide-based precursors, exemplified by the ALD using $Al_2Cl_6$ with water[55] or with homoleptic alkoxide precursors as the co-reactant.[36,56] $Al_2Cl_6$ is of interest because it is relatively inexpensive, exhibits high volatility and undergoes fast reactions with OH surface groups. However, one of the main drawbacks of using halide-based precursors is the formation of corrosive HX (X = halide) reaction products, which can etch equipment parts as well as the forming film, the latter leading to high surface roughness.[57] Other precursors include homoleptic $[Al(mmp)_3]$, which has been employed as an $Al_2O_3$ precursor using liquid-injection ALD;[58] however, the volatility of this precursor is not sufficiently high for more conventional vapor-phase delivery. $[Al(NEt_2)_3]_2$ has also been employed with water[59,60] and ozone,[61] affording a high growth per cycle (GPC) of ~1.3 Å/cycle. However, depositions were not reported below 200 °C, which is necessary for temperature-sensitive substrates.

Another possible alternative to TMA is the heteroleptic dimer $[Al(CH_3)_2(\mu\text{-O}^i\text{Pr})]_2$ (DMAI). The dimer is formed by the formation of a dative bond between the O atom in the $\text{O}^i\text{Pr}$ ligand and the Al center of the other molecule. This is much stronger than the three-center-two-electron bond found in TMA so the dimer should prevail at higher temperatures, which can help to reduce pyrophoricity. As only one branched alkoxide ligand per Al center is present, higher oligomers (than dimer) do not occur in the solution phase, as confirmed by NMR studies.[62] Additionally, gas-phase electron diffraction studies have shown that compounds analogous to DMAI, of the general formula $[Al(CH_3)_2(\mu\text{-OR})]_n$ (R = $CH_3$, $n = 3$; R = $C(CH_3)_3$, $n = 2$), retain their respective oligomeric form in the gas phase.[63,64] Therefore, it is assumed that DMAI also remains dimeric in the gas phase. The dimeric structure has also been observed intact on an Si(100) surface,[65] which may have (steric) consequences for the ALD process.

TABLE I. General properties of TMA and DMAI precursors. The vapor pressures of the precursors were measured as previously reported.[66]

| Precursor property | TMA | DMAI |
|---|---|---|
| Physical state (R.T.P.) | Liquid | Liquid |
| Melting point | 15 °C | <R.T. |
| Boiling point | 125 °C | 172 °C |
| Decomposition temperature | ~330 °C[94] | ~370 °C[65] |
| Vapor pressure | 9 Torr at 16.8 °C | 9 Torr at 66.5 °C |
| Pyrophoric | Yes | No |

Note: R.T. = room temperature.

The general properties of TMA and DMAI are compared in Table I. Both compounds are liquid at room temperature, which facilitates handling. Differences between the two compounds are more pronounced at higher temperatures, as DMAI has a higher boiling point than TMA. However, the onset of decomposition for DMAI occurs at approximately 50 °C higher than TMA, showing that DMAI is the more stable molecule of the two, which is beneficial for ALD precursors. The open-crucible TGA plot of DMAI (Fig. 1) showed a rapid drop in mass of one step. The residual mass was very low, <0.3%, which is indicative of evaporation rather than (significant) decomposition taking place at this temperature. The onset of evaporation occurred at a higher temperature than that for TMA, suggesting that the vapor pressure of DMAI was lower, which was corroborated with vapor pressure measurements. DMAI afforded a vapor pressure of ~9 Torr (~1.2 kPa) at 66.5 °C (measured as previously

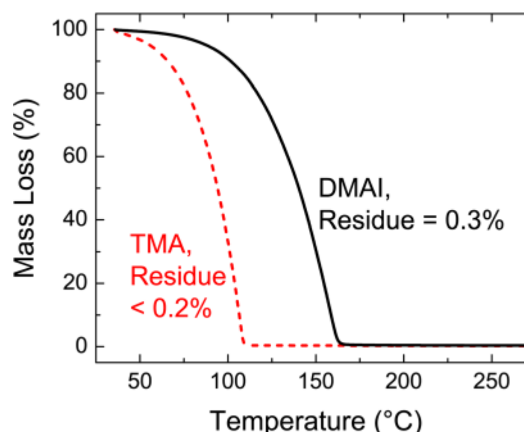


FIG. 1. (Color online) Thermogravimetric analysis (TGA) curves for DMAI and TMA (open-crucible). The TGA was carried out at atmospheric pressure using a Seiko Instruments TG-DTA instrument at a heating rate of 10 °C $min^{-1}$ under a flow of $N_2$ (99.999%, 30 sccm).

reported[66]), which was lower than that of TMA (9 Torr at 16.8 °C). The lower vapor pressure is most likely to be due to the dimerization of DMAI, which is facilitated by the $O^iPr$ ligand. Nevertheless, this dimerization leads to a stable, non-pyrophoric, and potentially safer compound for use as a precursor, making DMAI a promising possible alternative to TMA.

## III. EXPERIMENT

### A. Atomic layer deposition

The experiments were carried out on an Oxford Instruments OpAL$^{TM}$ reactor located in a clean-room. It is an open-load system, which operates with a rotary pump and features a remote inductively-coupled plasma source. The base pressure was ~1 mTorr and typical operating pressures were 100–500 mTorr. DMAI (99.999%) was provided by Air Liquide, France. Data from our previous ALD work[17] with TMA (Air Liquide, 99.9999%) were used for the process comparison. The DMAI was held in a stainless steel bubbler at 60 °C and Ar (>99.999%, 50 sccm) was used as a carrier gas. For plasma-enhanced ALD, oxygen and argon (both purity >99.999%) were flowed into the reaction chamber at 50 and 20 sccm, respectively, throughout the process as DMAI was not found to react with oxygen under these conditions. The RF plasma power was 150 W. Argon alone was used to purge the precursor lines. For the thermal ALD process, water (VWR, GBR Rectapur grade, >99.999%) was held in a water-cooled stainless steel bubbler at 19 °C to reduce the vapor pressure and prevent overdosing. Argon (200 sccm) alone was used as a continuous process gas for the thermal ALD experiments (the argon for DMAI bubbling remained at 50 sccm). The saturation curves were obtained at a substrate temperature of 150 °C. For the temperature series, longer purges than necessary (10 s) were used to exclude parasitic CVDlike reactions over the full temperature range. The ALD step times (DMAI dose–purge–co-reactant–purge) were as follows: plasma-enhanced ALD ($O_2$ plasma), 0.5–10–4–10 s; thermal ALD ($H_2O$), 0.5–10–0.03–10 s. Films for the temperature series were deposited using 500 ALD cycles. The GPC was then calculated by dividing the overall thickness (measured by spectroscopic ellipsometry) by the number of cycles. The temperature ranges studied were 25–400 °C for plasma-enhanced ALD and 100–400 °C for thermal ALD.

### B. Analytical techniques

Film thicknesses were obtained by *in situ* and *ex situ* spectroscopic ellipsometry (SE) carried out on a J. A. Woollam M2000U (*in situ*) and M2000 D (*ex situ*) rotating compensator ellipsometers. The latter was mounted on a multiangle Gonio stage (angles used: 65, 70, 75, and 80°). Modeling was carried out using CompleteEASE software. The model layers comprised Si, native $SiO_2$ and $Al_2O_3$. The $Al_2O_3$ layer was modeled using a Cauchy layer over a wavelength range of 190–1000 nm (1.2–6.5 eV). Further details on the SE technique and modeling can be found in the literature.[67] The atomic composition (areal density) of the films was obtained at AccTec using Rutherford backscattering spectrometry (RBS) with 2 MeV $^4He^+$ ions, except for the hydrogen content, which was obtained on the same apparatus using elastic recoil detection (ERD).

Quadrupole mass spectrometry (QMS) was conducted using a Pfeiffer Vacuum QMS 200 (electron energy = 70 eV) with channeltron detector, which was connected to the deposition chamber via a heated pipeline (80 °C) and a 150 $\mu$m pinhole. The base pressure in the differentially-pumped QMS chamber was $\sim 10^{-6}$ Torr although this typically rose to $\sim 10^{-5}$ Torr during measurements. ALD purges were extended to 30 s (after DMAI dose) and 15 s (after water or plasma dose) for these measurements. Measurements where only the DMAI was introduced into the chamber, and separate measurements for $O_2$ plasma only, and water only were made prior to measuring the full ALD cycles for reference purposes and to correct for pressure effects.

XPS measurements were performed on a Thermo Scientific K-Alpha KA1066 spectrometer using a monochromatic Al K$\alpha$ X-ray source ($h\nu = 1486.6$ eV). Photoelectrons were collected at a take-off angle of 60°. An X-ray spot 100 $\mu$m in diameter was used in the analyses. The samples were neutralized using a flood gun to correct for differential or non-uniform charging. All spectra were corrected for sample charging using the Al 2*p* peak in $Al_2O_3$ (binding energy = 74.4 eV)[68] as an internal reference. High-resolution XPS scans were performed for the Al 2*p*, O 1*s*, C 1*s*, and Si 2*p* regions at a pass energy of 50 eV.

## IV. RESULTS AND DISCUSSION

### A. ALD process

The initial DMAI process was based on the TMA process used in the OpAL$^{TM}$ reactor, which was reported earlier.[17] Hereafter, plasma-enhanced ALD refers to the use of a remote $O_2$ plasma as the co-reactant and thermal ALD refers to water as the co-reactant. The DMAI bubbler temperature was set to 60 °C. Bubbler temperatures of 70 °C and 80 °C were also tested but were found to have no significant influence on the GPC of $Al_2O_3$ in the OpAL$^{TM}$ system. For the plasma-enhanced process, the purges were set to 10 s while the DMAI dose and plasma exposure were varied independently. DMAI saturation, carried out at a substrate temperature of 150 °C, was observed at doses $\leq$0.5 s (Fig. 2), both with Ar bubbling and a vapor draw. TMA typically saturates at <50 ms under these conditions.[17] As the former afforded a higher GPC, bubbling was retained for the remaining experiments. The plasma dosing time (not shown) saturated after 2 s of plasma exposure. The purging times were also optimized for a 0.5 s DMAI dose at a substrate temperature of 150 °C. The post-DMAI purge was found to saturate after 3 s, below which significant CVD-like reactions occurred. The post-plasma purge tests showed no variation in GPC with dosing time, suggesting that the post-plasma purge was not a key parameter in the DMAI process, which is in agreement with other plasma-enhanced ALD processes.[16] Purging times were not optimized for other substrate temperatures so all purge times were set to 10 s for the temperature series

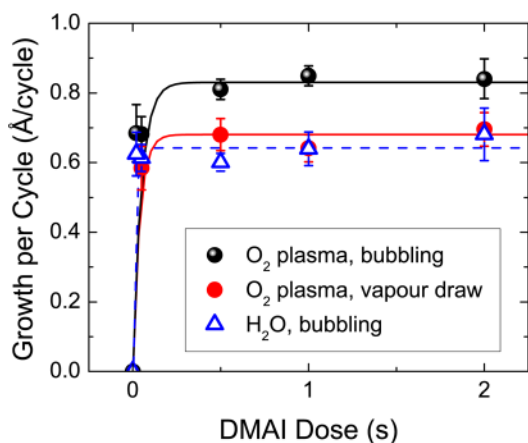


FIG. 2. (Color online) Saturation curves for the DMAI dose for plasma-enhanced ALD with and without DMAI bubbling (Ar, 50 sccm) and thermal ALD with bubbling. Lines serve as a guide to the eye.

investigations to exclude any possible influence of CVD-like reactions. For thermal ALD, the DMAI dose (with Ar bubbling, Fig. 2) was found to saturate at 50 ms, but standard dosing times were maintained at 0.5 s for comparison with the plasma-enhanced process. Purging times were set to 10 s and the water dose was maintained at 30 ms. *In situ* SE of both the plasma-enhanced and thermal processes using these cycle times at 150 °C showed a linear increase in film thickness with each ALD cycle and no discernable nucleation delay (Fig. 3).

Quadrupole mass spectrometry (QMS) measurements (Fig. 4) were carried out at a substrate temperature of 150 °C. A cracking pattern of the DMAI precursor [Fig. 4(a)] was recorded to facilitate choosing which peaks to follow during the ALD processes. An intense peak was observed at $m/z = 116$, which corresponds to $[Al(CH_3)_2(O^iPr)]^+$ (the DMAI monomer). A less intense peak at $m/z = \sim 130$ was present, suggesting that some dimeric DMAI was also present, although analysis of higher $m/z$ values was beyond the range of the QMS apparatus. A series of peaks for lower $m/z$ values, corresponding to sequential loss of $CH_3$ moieties, were also present. Additionally, the intensities of $m/z = 10$–$60$ were higher than the background measurement when DMAI was introduced into the reactor, confirming that they were present as a result of the precursor. For the purpose of ALD cycle analysis, the signals for $m/z = 15$ ($CH_3^+$, used to follow $CH_4$ in order to avoid confusion with $O^+$ at $m/z = 16$), 28 ($CO^+$ or hydrocarbon ions), 44 ($CO_2^+$ mainly, and hydrocarbon ions), 60 ($HO^iPr^+$) were followed; in addition to $m/z = 116$ for the DMAI monomer. Prior to the full measurements, ALD half-cycles were analyzed for reference purposes, where each individual precursor was repeatedly introduced into the reaction chamber without co-reactants. Each half-cycle is referred to as DMAI-only, $O_2$-plasma-only and $H_2O$-only.

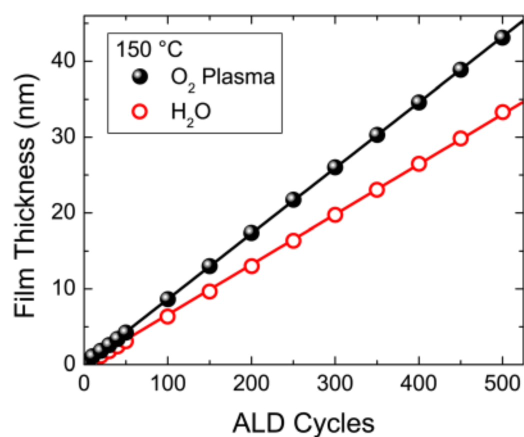


FIG. 3. (Color online) Increase of $Al_2O_3$ thickness as a function of ALD cycles, measured using *in situ* spectroscopic ellipsometry, showing a linear increase in thickness with the number of cycles with no nucleation delay.

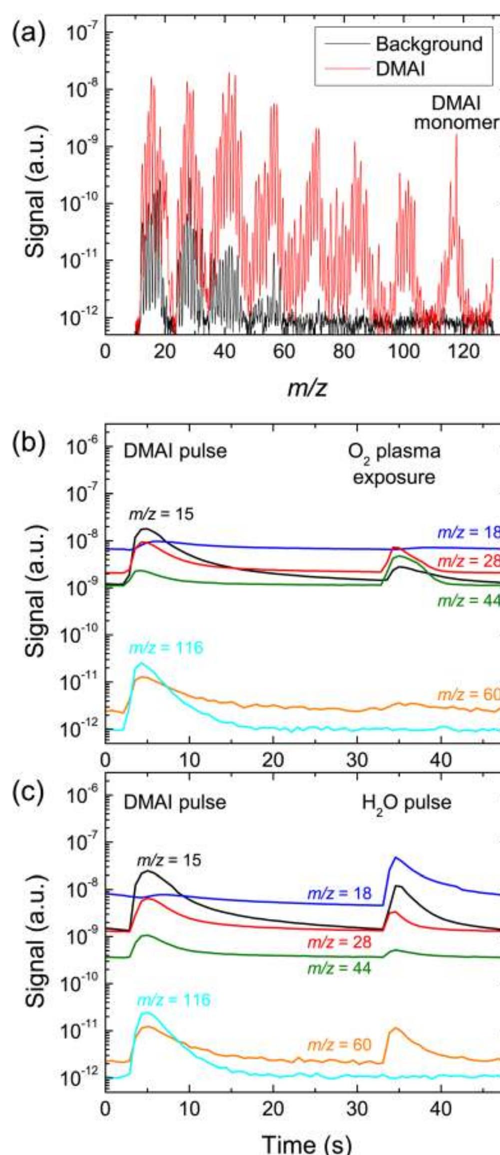


FIG. 4. (Color online) Quadrupole mass spectrometry (QMS) results for DMAI at 150 °C. (a) DMAI cracking pattern and QMS profiles for (b) plasma-enhanced and (c) thermal DMAI ALD processes. The masses were assigned as follows: $m/z = 15$, $CH_3^+$ (for following $CH_4$ and fragments of $HO^iPr$ and DMAI); $m/z = 18$, $H_2O^+$; $m/z = 28$, $CO^+$ or $CH_x^+$ (from $HO^iPr$ or DMAI cracking); $m/z = 44$, $CO_2^+$ or $CH_x^+$ (from $HO^iPr$ or DMAI cracking); $m/z = 60$, $HO^iPr^+$, and $m/z = 116$, $[Al(CH_3)_2(O^iPr)]^+$ (DMAI monomer).

A full plasma-enhanced ALD cycle using DMAI is shown in Fig. 4(b). Looking at the DMAI pulse half-cycle, it can be seen that the introduction of DMAI ($m/z = 116$) into the chamber resulted in an increase in all the masses studied. Firstly, the relatively weak signal increase of $m/z = 18$ ($H_2O^+$) is most likely to be due to a pressure effect. Comparing the increases of $m/z = 28$ and 44 with the increase in $m/z = 116$ during the DMAI pulse, the ratios of these increases were higher than those observed in the DMAI-only half cycle, which suggests that $m/z = 28$ and 44 are the result of hydrocarbon cracking products of $HO^iPr$, as well as the DMAI, rather than reaction products. For $m/z = 15$ ($CH_3^+$) and $m/z = 60$ ($HO^iPr^+$), the increases in the signals were stronger than for the DMAI-only cycles, suggesting that $CH_4$ and $HO^iPr$ are formed as the reaction products, which is consistent with previous reports in the literature for DMAI[69] and for TMA.[70] Therefore, the most likely simultaneous surface reactions occurring during the DMAI dose are represented by Eqs. (1a) and (1b):

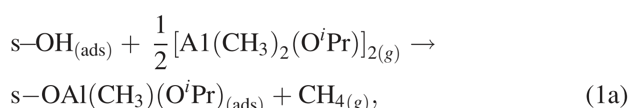

$$\text{s–OH}_{(ads)} + \frac{1}{2}[\text{Al}(\text{CH}_3)_2(\text{O}^i\text{Pr})]_{2(g)} \rightarrow \text{s–OAl}(\text{CH}_3)(\text{O}^i\text{Pr})_{(ads)} + \text{CH}_{4(g)}, \quad (1a)$$

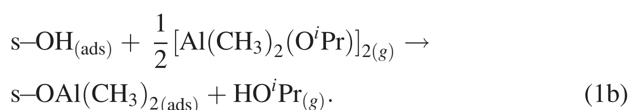

$$\text{s–OH}_{(ads)} + \frac{1}{2}[\text{Al}(\text{CH}_3)_2(\text{O}^i\text{Pr})]_{2(g)} \rightarrow \text{s–OAl}(\text{CH}_3)_{2(ads)} + \text{HO}^i\text{Pr}_{(g)}. \quad (1b)$$

Surface-bound species are denoted by "s". These and all subsequent reaction equations [Eqs. (2) and (3)] show monofunctional reactions between the incoming reactants and the surface, although bi-functional reactions are also possible,[71] as is common for TMA.

During the $O_2$ plasma exposure step [Fig. 4(b)], signal increases were observed for $m/z = 28$ and 44, which is consistent with the formation of $CO_2$ as a result of the $O_2$ plasma undergoing combustion-like reactions with the alkyl ligands on the surface.[16] The intensity ratio of the $CO_2^+$:$CO^+$ signals was 1:1.4, which is consistent with the formation of $CO^+$ as a result of the plasma rather than simply the cracking of $CO_2^+$ by electron ionization in the QMS chamber (which would give a ratio of ~1:0.1).[72] The signal for $m/z = 18$ was very weak, despite $H_2O$ being expected as a product for combustion-like reactions[16] as has been observed during plasma-enhanced ALD using TMA.[70] The weak signal is most likely a result of the high baseline for $m/z = 18$. Moreover, the evolution of $m/z = 18$ appears to start after $m/z = 15$, 28, and 44, suggesting that any water produced remains in the reactor or cannot reach the QMS detector within the time-frame of the experiment. There appeared to be a slight increase in the signal for $m/z = 60$, accounting for $HO^iPr$ formation, the cracking of which might also contribute to the $m/z = 15$, 28, and 44 signals. This peak was not observed during the $O_2$-plasma-only cycles. The peak for $m/z = 60$ was substantially less prominent than that observed during the $H_2O$ dose in thermal ALD [Fig. 4(c)], suggesting that much less $HO^iPr$ evolves, if any at all, during the $O_2$ plasma exposure. Either $HO^iPr$ is not formed as full combustion occurs on the surface, meaning that the peak resulted from a pressure effect, or it is formed by the reaction of surface $O^iPr$ with $H_2O$ produced by the aforementioned combustion (which would also account for the low $m/z = 18$ signal), but it is then combusted in the gas phase before reaching the spectrometer. Additionally, it is known that $O_2$ plasma exposures result in a higher concentration of surface OH than $H_2O$ exposures.[44] Therefore, more ligands can potentially react during the subsequent DMAI step, leaving less surface $O^iPr$ to react with the following plasma exposure and therefore creating less $HO^iPr$ than with thermal ALD. Taking these observations into account, and assuming that full combustion takes place at the surface, two simultaneous reactions [Eqs. (2a) and (2b)] are likely to be taking place:

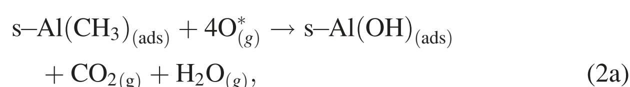

$$\text{s–Al}(\text{CH}_3)_{(ads)} + 4\text{O}^*_{(g)} \rightarrow \text{s–Al}(\text{OH})_{(ads)} + \text{CO}_{2(g)} + \text{H}_2\text{O}_{(g)}, \quad (2a)$$

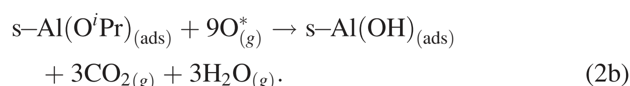

$$\text{s–Al}(\text{O}^i\text{Pr})_{(ads)} + 9\text{O}^*_{(g)} \rightarrow \text{s–Al}(\text{OH})_{(ads)} + 3\text{CO}_{2(g)} + 3\text{H}_2\text{O}_{(g)}. \quad (2b)$$

An asterisk denotes a plasma.

For thermal ALD [Fig. 4(c)], the QMS signals during the DMAI dose are almost identical to those of the DMAI dose for plasma-enhanced ALD; therefore, Eq. (1a) and (1b) also hold for the DMAI dose in thermal ALD. During the water dose (shown by the increase in $m/z = 18$, $H_2O^+$), increases in the signals for $m/z = 15$ ($CH_3^+$) and 60 ($HO^iPr^+$) suggest the production of $CH_4$ and $HO^iPr$ with $m/z = 28$ and 44 accounting for cracking products of the latter. Therefore, the following simultaneous reactions [Eq. (3a) and (3b)] are likely to be taking place:

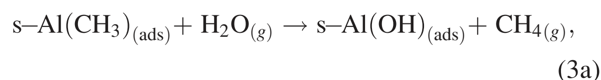

$$\text{s–Al}(\text{CH}_3)_{(ads)} + \text{H}_2\text{O}_{(g)} \rightarrow \text{s–Al}(\text{OH})_{(ads)} + \text{CH}_{4(g)}, \quad (3a)$$

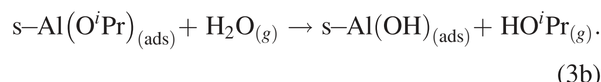

$$\text{s–Al}(\text{O}^i\text{Pr})_{(ads)} + \text{H}_2\text{O}_{(g)} \rightarrow \text{s–Al}(\text{OH})_{(ads)} + \text{HO}^i\text{Pr}_{(g)}. \quad (3b)$$

The QMS data support the situation where DMAI reacts with a hydroxylated surface in a similar manner to TMA, via ligand-exchange reactions during thermal ALD with the addition of combustion-like reactions during plasma-enhanced ALD using an $O_2$ plasma.

To investigate the ALD behavior of DMAI as a function of temperature, both plasma-enhanced and thermal ALD using DMAI were carried out at 25–400 and 100–400 °C, respectively. These temperature ranges correspond to those investigated with TMA in the Oxford Instruments OpAL™ reactor.[17] A selection of film properties at 200 °C are presented in Table II. For the plasma-enhanced ALD using DMAI, a much flatter GPC profile (Fig. 5) was observed than that for TMA, with a reasonably constant GPC of ~0.85 Å/cycle, as measured by SE. At 25 °C, a slight increase

TABLE II. Properties of $Al_2O_3$ deposited onto Si wafers by ALD using DMAI and TMA at 200 °C in an Oxford Instruments OpAL™ reactor.

| Plasma-enhanced ALD | TMA | DMAI |
|---|---|---|
| Growth per cycle | 1.18 ± 0.01 Å/cycle | 0.85 ± 0.05 Å/cycle |
| Al atoms per cycle | 4.3 ± 0.5 at. $nm^{-2}$ $cycle^{-1}$ | 2.4 ± 0.1 at. $nm^{-2}$ $cycle^{-1}$ |
| [O]/[Al] ratio | 1.5 ± 0.1 | 1.8 ± 0.1 |
| [H] | 2.5 ± 0.2 at. % | 7.0 ± 0.5 at. % |
| Mass density | 3.1 ± 0.2 g $cm^{-3}$ | 2.6 ± 0.2 g $cm^{-3}$ |
| Refractive index (630 nm) | 1.66 ± 0.02 | 1.62 ± 0.02 |
| **Thermal ALD** | **TMA** | **DMAI** |
| Growth per cycle | 1.01 ± 0.01 Å/cycle | 0.93 ± 0.05 Å/cycle |
| Al Atoms per cycle | 3.7 ± 0.4 at. $nm^{-2}$ $cycle^{-1}$ | 2.6 ± 0.1 at. $nm^{-2}$ $cycle^{-1}$ |
| [O]/[Al] ratio | 1.5 ± 0.1 | 1.7 ± 0.1 |
| [H] | 2.7 ± 0.2 at. % | 14.7 ± 1.0 at. % |
| Mass density | 2.9 ± 0.2 g $cm^{-3}$ | 2.6 ± 0.2 g $cm^{-3}$ |
| Refractive index (630 nm) | 1.65 ± 0.02 | 1.60 ± 0.02 |

in GPC was observed. For TMA, the reduction in GPC with increasing temperature was an indication of dehydroxylation: the thermally-driven loss of two surface OH groups via the release of water vapor.[17,73] For thermal ALD, a rapid increase in GPC was observed with increasing temperature over the range 100–250 °C. This change was more pronounced than that observed for the TMA. At 250 and 300 °C, a higher GPC was obtained than that with TMA.

For a clearer picture of the behavior, it is better to look at the number of Al atoms deposited per cycle [Fig. 6(a)],[17] because the GPC is affected by many factors, including film density. It is clear that approximately half the number of Al atoms was deposited during the plasma-enhanced ALD of DMAI than with TMA (for example, 4.3 and 2.4 at. $nm^{-2}$ $cycle^{-1}$, respectively, at 200 °C). Over the temperature ranges for both plasma-enhanced and thermal ALD using DMAI, the Al atoms deposited increased with increasing deposition temperature, which is indicative of an influence of thermal activation being required during the precursor dosing step. With respect to thermal ALD, the increase in atoms with temperature for DMAI was much more pronounced than that for TMA, indicating the extra thermal energy required for reaction. The presence of the $O^iPr$ ligand and the fact that the Al–O bonds have a higher bond energy than Al–C bonds is the most likely cause for this. Therefore, the $O^iPr$ ligand requires more thermal energy to react with s-OH than $CH_3$.

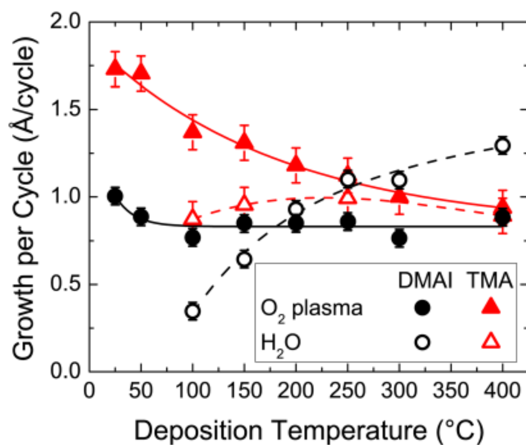


FIG. 5. (Color online) Growth per cycle as a function of deposition temperature for the plasma-enhanced and thermal ALD of $Al_2O_3$ using DMAI and TMA as precursors. Lines serve as a guide to the eye.

In addition to the reaction kinetics, steric hindrance is also likely to influence the number of Al atoms deposited. Neglecting the dimeric nature of the DMAI, it has also been reported that alkoxide ligands block OH surface sites,[74] which may also account for the drop in Al atoms deposited with decreasing temperature, and the lower number of Al atoms deposited in general using DMAI instead of TMA. Investigations by Yanguas-Gil and Elam into the control of GPC (and hence the number Al atoms deposited) using alcohols in the TMA/$H_2O$ process showed that the addition of a $HO^iPr$ step in the ALD cycle reduced the GPC to ∼52% of its original value.[75] Therefore, in the case of ALD using DMAI, when the initial DMAI molecules have chemisorbed to the surface, they can effectively shield any remaining OH surface sites from remaining incoming molecules, i.e., saturation is reached with fewer Al atoms deposited compared with TMA. The work of Yanguas-Gil also demonstrated that the surface $O^iPr$ could be easily removed with a water pulse, so it is expected that the $O^iPr$ ligand has the greatest influence on the growth during the DMAI pulse.

## B. Film composition

Figures 6(b) and 6(c) compare the O/Al ratio and H content of the films deposited using DMAI and TMA. Where DMAI was the precursor, the O/Al ratio decreased with increasing substrate temperature in a similar trend to that for the films from TMA. However, the O/Al ratio for the films from DMAI (plasma-enhanced or thermal ALD) was always slightly higher than that for the corresponding TMA process. There was not a significant difference at substrate temperatures of 150 °C and above (1.6–1.8). At 25 and 100 °C the difference was more apparent. For the plasma-enhanced ALD samples at 25 °C, the O/Al ratio was as high as 3.1 for

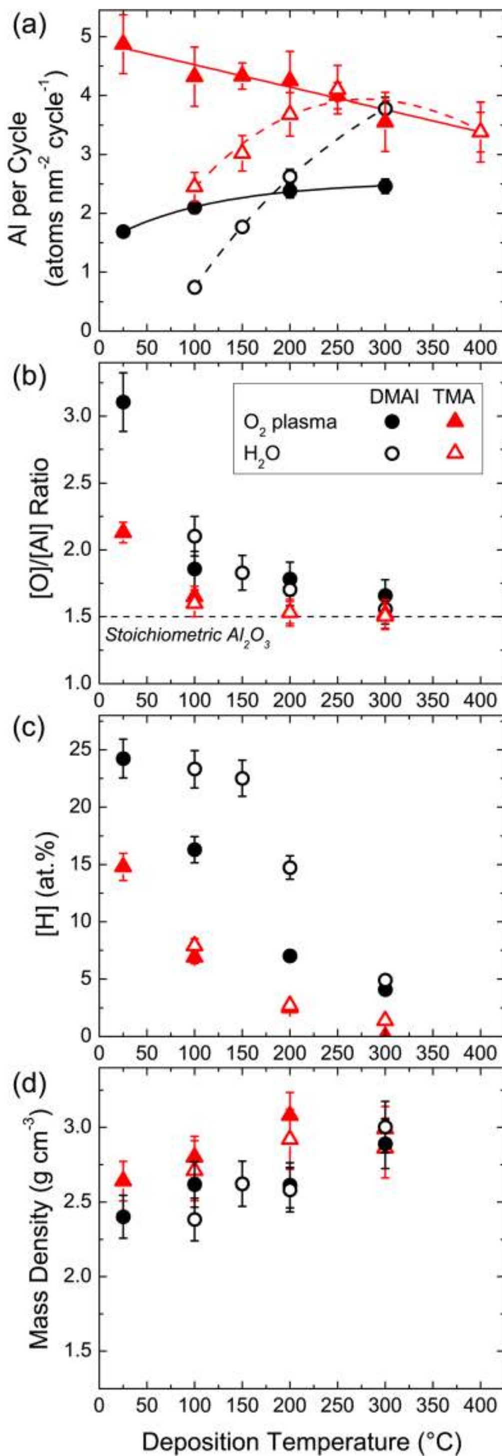


FIG. 6. (Color online) Film composition as a function of deposition temperature obtained using Rutherford backscattering spectrometry and elastic recoil detection. (a) The number of Al atoms deposited per cm$^2$ per cycle, (b) the O/Al ratio, (c) the H concentration, and (d) the mass density of the films. Lines serve as a guide to the eye.

DMAI, compared with 2.1 for TMA, which suggests that OH is not removed as easily as in the case for TMA,[17] and that $O^iPr$ is easily incorporated at this temperature. ~9 at. % C was detected by RBS for the 25 °C film, implying an incorporation of carbonates, formates or similar carbon species. Additionally, the H content of the DMAI films was also higher, in some cases twice the value of the films from TMA. The incorporation of more H, C, and O using DMAI is consistent with the thermal activation required for reaction with surface groups when compared with TMA, and $O^iPr$ is thereby easily incorporated in the films. Additionally, it is known that aluminum mono- or di-alkoxide precursors can result in higher oxygen content for CVD films.[76] Yamashita *et al*. showed that this incorporation of O into a TMA molecule increased the O/Al ratio in $AlO_x$ films deposited by CVD and that this was related to the concentration of $O_2$ gas,[77] which suggested that O was more easily incorporated into the film when formally bound to the metal in an alkoxide (or peroxide) compound. It is therefore highly plausible that the $O^iPr$ ligand in DMAI is more easily incorporated into the growing film as OH and C, particularly at lower deposition temperatures. It is this OH and C incorporation that is the likely cause for the lower $Al_2O_3$ densities afforded by DMAI than those by TMA [Fig. 6(d)]. For DMAI, the film densities ranged from 2.4–3.0 g cm$^{-3}$, which were slightly lower than the 2.6–3.1 g cm$^{-3}$ for the films from TMA. In every case, the films deposited using plasma-enhanced ALD had higher densities than thermal ALD at the same temperatures. Additionally, the film density increased with increasing deposition temperature, which coincides with the reductions in O/Al ratio and H content.

In order to better understand the nature of the elements present in the films, XPS studies were conducted. Depth profiles (Fig. 7) confirmed that the O and Al contents were consistent throughout the 'bulk' of the films. Figure 7(a) shows the depth profile of a film deposited at 200 °C by plasma-enhanced ALD, which is representative of the films deposited by plasma-enhanced ALD at 100 °C and above, and by thermal ALD at 150 °C and above. C was only observed at the film surface, which is a result of contamination from the ambient. It was only the films deposited by plasma-enhanced ALD at 25 °C [Fig. 7(b)] that showed ~5 at. % C throughout the film. The effect of C and OH incorporation on film density [see also Fig. 6(d)] was also supported by the shorter sputtering time required to reach the interface. For example, the film deposited at 200 °C [Fig. 7(a)] resulted in a sputtering rate of 0.35 nm s$^{-1}$, whereas, for the film deposited at 25 °C [Fig. 7(b)] a sputtering rate of 0.56 nm s$^{-1}$ was observed. The higher sputtering rate for the sample deposited at 25 °C is indicative of a film with a lower density (corroborated by the mass density data), caused by the incorporation of C and OH.

To assess the environments of the elements in the film, the binding energies of the Al 2*p* and C 1*s* peaks were analyzed. Si 2*p* peaks were also analyzed, showing an $SiO_2$ environment only at the film-substrate interface, and no silicate environments as observed with direct plasma ALD.[20] The O 1*s* peak did not give any useful information as the binding energies for many O-containing environments are very similar.[68] To discount the effect of any surface carbon, the data from 20 s sputtering time were analyzed. For the plasma-enhanced ALD samples, only a singular Al 2*p* peak was observed for films deposited at 100 °C and above (films synthesized at 50 °C were not analyzed by XPS). Figure 8(a) is an example of the Al 2*p* peak at 200 °C. For these

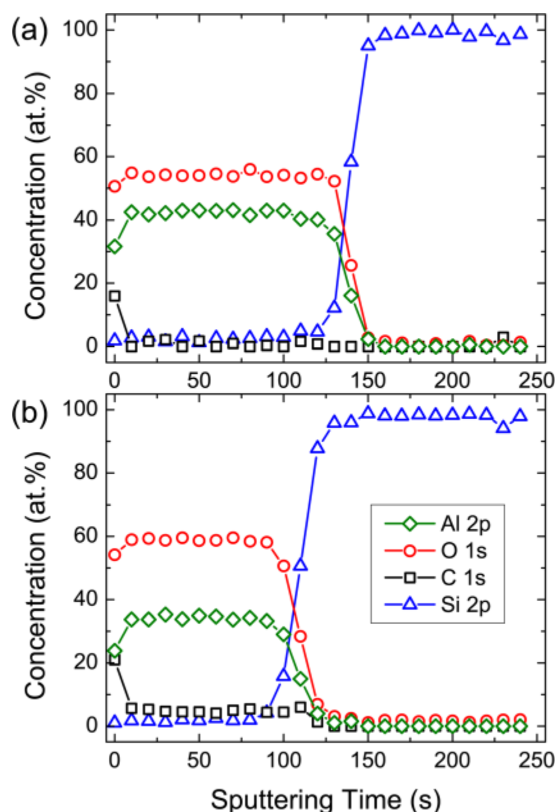


FIG. 7. (Color online) XPS depth profiles of $Al_2O_3$ films deposited by plasma-enhanced ALD using DMAI at (a) 200 °C (42.5 nm thick) and (b) 25 °C (50.2 nm thick).

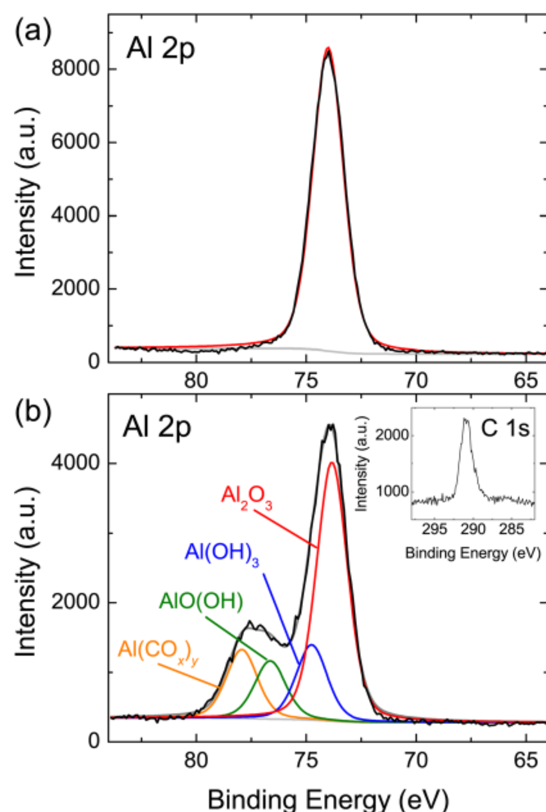


FIG. 8. (Color online) Al 2*p* peaks from the XPS spectra of $Al_2O_3$ films deposited by plasma-enhanced ALD using DMAI at (a) 200 °C, showing an oxide environment only, and (b) 25 °C, with evidence of $Al(OH)_3$ (hydroxyl), AlO(OH) (oxyhydroxyl) and $Al(CO_x)_y$ (carbonate) species. Inset: the C 1*s* peak observed in films deposited at 25 °C, indicative of carbonate species.

substrate temperatures, the C 1*s* peak was not observed at this sputtering time. For the 25 °C sample [Fig. 8(b)], a shoulder peak centered at ~78 eV was present in addition to the main $Al_2O_3$ peak. These peaks were deconvoluted to three Al environments in addition to $Al_2O_3$, which were assigned to $Al(OH)_3$, AlO(OH), and $Al(CO_x)_y$ species,[78] the latter species being confirmed by the C 1*s* peak at ~291 eV [inset, Fig. 8(b)]. The hydroxyl-based environments are expected at such low deposition temperatures,[17,73] as OH is more easily incorporated into the film. The carbonates and related species are generally considered to be a transient species in the formation of $CO_2$ as part of the TMA/$O_2$ plasma process,[79] rather than a more permanent feature of the films. C was also observed in $Al_2O_3$ films deposited by plasma-enhanced ALD using TMA at 25 °C,[45] although the exact nature of the C environment was not confirmed in that case.

For thermal ALD films deposited >100 °C, the nature of the Al 2*p* peak was the same as that for plasma-enhanced ALD [an example of the film deposited at 200 °C is given in Fig. 9(a)]. The only exception was at 100 °C [Fig. 9(b)], where $Al(OH)_3$ was observed as a slight shoulder to the $Al_2O_3$ peak. C was not observed by XPS in the bulk of the films at any temperature for thermal ALD.

Overall, the $Al_2O_3$ deposited at higher deposition temperatures (>150 °C), were comparable in composition to those deposited using TMA. It was only at the lower temperatures that significant differences were observed in terms of stoichiometry and composition.

In addition to film composition, the films' uniformity was examined. 500 ALD cycles of $Al_2O_3$ were deposited on a 200 mm Si wafer at 150 °C by both plasma-enhanced and thermal ALD using DMAI. The film thickness was measured at 1 cm intervals using spectroscopic ellipsometry to form a 2D matrix over the wafer, from which the percentage non-uniformity was calculated using Eq. (4).

$$\text{non-uniformity} = \left(\frac{d_{\max} - d_{\min}}{2d_{\text{average}}}\right) \times 100, \quad (4)$$

where $d$ is the film thickness. The non-uniformity values for films deposited by DMAI were 8.1% for plasma-enhanced ALD and 4.3% for thermal ALD, which were both higher than the respective 5.5 and 1.6% for TMA. However, it should be noted that the deposition parameters were the same as those for TMA and no steps were taken to optimize the process specifically for DMAI uniformity. The lower uniformity is attributed to the presence $O^iPr$ ligand, as alkoxide precursors are known to give films with a lower uniformity compared with more reactive ligands.[74] Elers *et al.* showed that ligands with low reactivity can reduce the uniformity of ALD films,[57] either by remaining on the surface (blocking reactive surface sites for subsequent precursor molecules) or by forming reaction products that can readsorb onto the surface and sterically shield surrounding surface groups. Compared with TMA, DMAI molecules have a

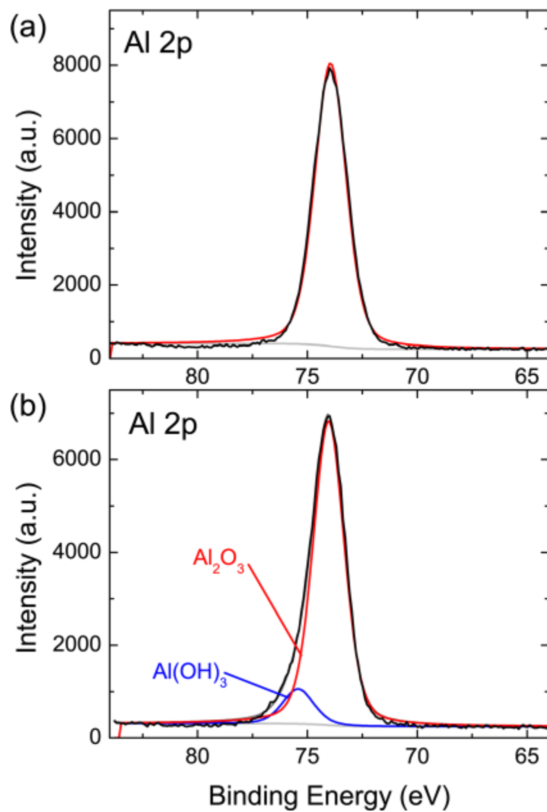


FIG. 9. (Color online) Al 2*p* peaks from the XPS spectra of $Al_2O_3$ films deposited by thermal ALD using DMAI at (a) 200 °C, showing an oxide environment only, and (b) 100 °C, with evidence of OH species.

greater (steric) surface area, especially if they remain as dimers on the surface. During the DMAI dose, the first molecules that react with the surface groups can shield more of the surface than TMA, thereby blocking potential reactive sites, leading to a lower uniformity. Other causes of non-uniformity can occur during the $H_2O$ dose (thermal ALD), where $O^iPr$ ligands give $HO^iPr$ as a reaction product [Eq. 3(b)], which may readsorb to vacant coordination sites on surface Al atoms, as has been observed for $TMA/H_2O$.[80,81] A similar effect was demonstrated in the aforementioned study by Yanguas-Gil,[59] where the GPC of various ALD processes was reduced by adding a pulse of an alkyl alcohol after the water dose. This method offered a high degree of process control and therefore led to uniform layers, whereas the concentration of $O^iPr$ on the surface originating form a DMAI molecule is more likely to be random and harder to control, leading to a higher degree of non-uniformity than observed with TMA.

## V. PASSIVATION OF SILICON SURFACES

Crystalline silicon solar cells benefit from a dielectric coating on their surfaces in order to reduce the loss of charge carriers through recombination at defect sites, such as dangling bonds.[4] $a$-$SiN_x$:H,[4,82–85] $SiO_2$,[86–89] and $Al_2O_3$[5–8] are popular materials for this application. $Al_2O_3$ has been of recent interest as an alternative to $SiO_2$ or $a$-$SiN_x$:H because $Al_2O_3$ films afford low recombination velocities on *n*- and *p*-type Si; for example, 2 and 13 cm $s^{-1}$, respectively,[5] where plasma-enhanced ALD using TMA was the deposition method. In addition to chemical passivation, $Al_2O_3$ exhibits a fixed negative charge at the Si interface, which induces field-effect passivation.[90]

In order to evaluate the passivation properties of the $Al_2O_3$ films from DMAI, 30 nm thick films were deposited on double-side-coated *n*-type (∼3.5 Ω cm) and *p*-type (∼2 Ω cm) floatzone Si wafers using plasma-enhanced ALD at 200 °C. For these Si wafers, the effective lifetime ($\tau_{eff}$) of the minority charge carriers within the Si reflects the level of passivation afforded by the thin film, where higher values of $\tau_{eff}$ indicate better passivation of the surface. $\tau_{eff}$ was determined by the photoconductance decay method in the transient mode and quasi-steady-state-mode (for $\tau_{eff} < 100\,\mu s$) using a Sinton lifetime tester (WCT 100). The surface passivation can also be represented by the surface recombination velocity ($S_{eff}$). The maximum surface recombination velocity ($S_{eff,max}$) was calculated from the $\tau_{eff}$ value,[6,9] using the expression

$$S_{eff,max} = \frac{d_W}{2\tau_{eff}}, \quad (5)$$

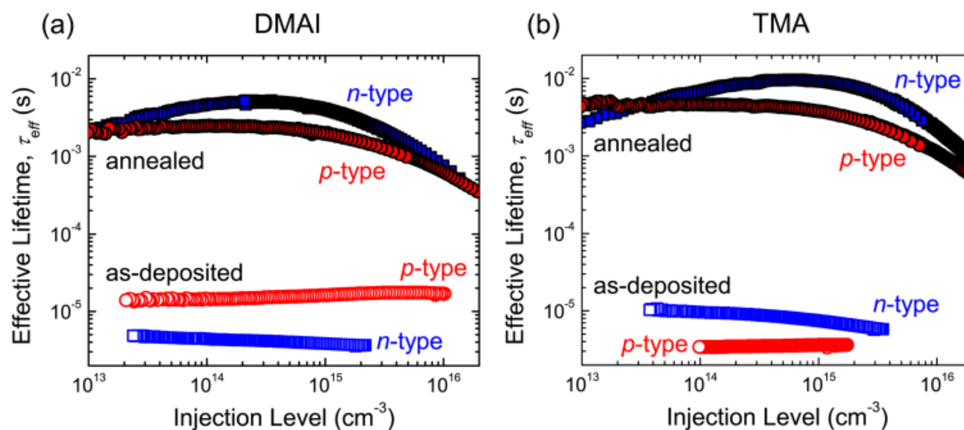


FIG. 10. (Color online) Effective lifetime ($\tau_{eff}$) of the minority charge carriers as a function of injection level for double-side-polished *n*- and *p*-type floatzone Si wafers (∼3.5 and ∼2 Ω cm, respectively) coated on both sides with 30 nm $Al_2O_3$ by plasma-enhanced ALD using (a) DMAI and (b) TMA at 200 °C.[9] Data are shown for the as-deposited films and films annealed for 10 min at 400 °C under $N_2$.

where $d_W$ is the thickness of the Si wafer ($\sim$280 $\mu$m). This calculation was based on the common assumption that all recombination takes place at the surface and not in the bulk of the floatzone wafer. $S_{eff,max}$ is reported at an injection level of $5 \times 10^{14}$ cm$^{-3}$. Annealing was found to be crucial for the improvement of Si surface passivation by $Al_2O_3$ films deposited using TMA.[9] Therefore, annealing was performed here using the same conditions used for the films deposited using TMA: 400 °C for 10 min under $N_2$.

The passivation properties of the $Al_2O_3$ films synthesized by plasma-enhanced ALD are shown in Fig. 10. As-deposited films prepared using DMAI [Fig. 10(a)] gave $\tau_{eff}$ values of $\sim$4 and $\sim$15 $\mu$s for *n*- and *p*-type Si, respectively, and $S_{eff,max}$ values were calculated to be in the order of $10^3$ cms$^{-1}$. These $\tau_{eff}$ values were low and $S_{eff,max}$ values high, but expected of as-deposited films. These values were also comparable to those reported for plasma-enhanced ALD using TMA as the Al precursor [Fig. 10(b)] under the same conditions.[5,9,90,91] After annealing, $\tau_{eff}$ improved significantly to $\sim$10 ms. Although these values were still slightly lower than those obtained with TMA under identical conditions, the level of surface passivation was still excellent. $S_{eff}$ values of <3 cm s$^{-1}$ and <6 cm s$^{-1}$ were obtained for *n*- and *p*-type Si, respectively, which are comparable to those reported for plasma-enhanced ALD using TMA as the Al precursor.[5,9,90,91] Additionally, the effective lifetimes obtained were higher than those reported for $Al_2O_3$ deposited by plasma-enhanced CVD[92] and RF sputtering.[93] The excellent passivation properties of the $Al_2O_3$ films can be attributed to a low interface defect density of $\leq 10^{11}$ eV$^{-1}$ cm$^{-2}$ and effective field-effect passivation.[90] In summary, $Al_2O_3$ from plasma-enhanced ALD using DMAI afforded effective carrier lifetimes ($\tau_{eff}$) which were comparable to similar films deposited using TMA.

## VI. SUMMARY AND CONCLUSIONS

Thin films of $Al_2O_3$ were deposited by remote plasma-enhanced ($O_2$ plasma) and thermal ($H_2O$) ALD using $[Al(CH_3)_2(\mu\text{-}O^iPr)]_2$ (DMAI) as an Al precursor. These depositions were compared with ALD using $[Al(CH)_3]$ (TMA) in the same reactor under nearly identical operating conditions. DMAI was shown to have good saturation characteristics and a constant increase in film thickness as a function of ALD cycles and no significant nucleation delay. Quadrupole mass spectrometry (QMS) data confirmed that $CH_4$ and $HO^iPr$ were reaction products during the DMAI dose for both plasma-enhanced and thermal ALD. Combustion-like products ($CO_2$ and some $H_2O$) were observed during the $O_2$ plasma dose, whereas $CH_4$ and $HO^iPr$ were observed during the $H_2O$ dose.

For plasma-enhanced ALD, the GPC obtained was 0.7–0.9 Å/cycle, which was lower than the 1.0–1.7 Å/cycle afforded by TMA. For thermal ALD, the GPC was as high as 1.2 Å/cycle at substrate temperatures >200 °C; however, this dropped rapidly with decreasing temperature. The lower GPC was a result of almost half the number of Al atoms being deposited per cycle where DMAI was the precursor. The film compositions (O/Al ratio and H and C content) obtained using DMAI at temperatures $\geq$150 °C were similar to films from TMA at the same temperatures. The film densities and film uniformity (DMAI) were also marginally lower than those obtained with TMA. At lower deposition temperatures, significant differences between DMAI and TMA were apparent. For plasma-enhanced ALD at 25 °C, $\sim$9 at. % C was measured by RBS. $\sim$8 at. % C was observed for thermal ALD at 100 °C, which was attributed to surface carbon. Films from TMA contained no detectable carbon in this study. C was below the RBS detection limit (5 at. %) for all other films. XPS studies confirmed the presence of, AlO(OH) and $Al(CO_x)_y$ species in addition to $Al_2O_3$ for the film deposited by plasma-enhanced ALD at 25 °C, which accounted for the low film density. For thermal ALD (100 °C), only $Al(OH)_3$ species were detected.

It is clear that changing one ligand on a precursor can have a significant effect on the ALD process(es) and the resulting films. Many of the features of the DMAI ALD process can be attributed to the presence of the $O^iPr$ ligand. During the DMAI dose, the $O^iPr$ moiety can sterically shield any surrounding surface sites from remaining incoming precursor molecules. This leads to a reduced GPC, fewer Al atoms deposited per cycle, lower film density and potentially lower film uniformity. Additionally, $O^iPr$ ligands are less reactive than $CH_3$ as the Al–O bond requires more energy to break it than Al–C. These features mean that the retention of the $O^iPr$ ligand in the film is much more likely during the DMAI dose. Nevertheless, films from DMAI at deposition temperatures $\geq$150 °C had comparable compositions to those from TMA. The quality of the films was demonstrated as $Al_2O_3$ films from DMAI offered good passivation of *n*- and *p*-type floatzone Si wafers, with effective carrier lifetimes in the order of 10 ms after annealing. Surface recombination velocities of <3 and <6 cms$^{-1}$ were obtained for *n*- and *p*-type Si, respectively, which is comparable to TMA.

In summary, $Al_2O_3$ films synthesized by ALD using DMAI offer films of comparable composition to those deposited by TMA at temperatures $\geq$150 °C. Therefore, DMAI can be considered a suitable alternative to TMA at these temperatures. DMAI has a low pyrophoricity and is therefore safer to handle, making it an appealing alternative to TMA as an Al precursor. The suitability of DMAI as an alternative precursor was evidenced by the good passivation afforded by $Al_2O_3$ films from DMAI afforded at 200 °C.

## ACKNOWLEDGMENTS

This work is supported by NanoNextNL, a micro and nanotechnology programme of the Dutch ministry of economic affairs, agriculture and innovation (EL&I) and 130 partners. The authors thank T. Fernández Landaluce (TU/e) for the XPS measurements, W. Arnold Bik (AccTec) for the RBS/ERD measurements, S. Bordihn (Q-Cells) for the uniformity measurements, and W. Keuning, C. A. A. van Helvoirt, J. J. A. Zeebregts and M. J. F. van de Sande (all TU/e) for their technical assistance, support, and advice.

[1] M. M. Frank, G. D. Wilk, D. Starodub, T. Gustafsson, E. Garfunkel, Y. J. Chabal, J. Grazul, and D. A. Muller, Appl. Phys. Lett. **86**, 152904 (2005).

[2]D. I. Garcia-Gutierrez, D. Shahrjerdi, V. Kaushik, and S. K. Banerjee, J. Vac. Sci. Technol. B **27**, 2390 (2009).
[3]L. W. Shang, Z. Y. Ji, Y. P. Cheng, H. Wang, X. Liu, M. X. Han, and M. Liu, Sci. China Technol. Sci. **54**, 95 (2011).
[4]A. G. Aberle, Prog. Photovoltaics: Res. Appl. **8**, 473 (2000).
[5]B. Hoex, S. B. S. Heil, E. Langereis, M. C. M. van de Sanden, and W. M. M. Kessels, Appl. Phys. Lett. **89**, 042112 (2006).
[6]B. Hoex, J. Schmidt, P. Pohl, M. C. M. van de Sanden, and W. M. M. Kessels, J. Appl. Phys. **104**, 044903 (2008).
[7]P. Poodt, A. Lankhorst, F. Roozeboom, K. Spee, D. Maas, and A. Vermeer, Adv. Mater. **22**, 3564 (2010).
[8]J. Schmidt, A. Merkle, R. Brendel, B. Hoex, M. C. M. van de Sanden, and W. M. M. Kessels, Prog. Photovoltaics **16**, 461 (2008).
[9]G. Dingemans, R. Seguin, P. Engelhart, M. C. M. van de Sanden, and W. M. M. Kessels, Phys. Status Solidi RRL **4**, 10 (2010).
[10]S.-H. K. Park, J. Oh, C.-S. Hwang, J.-I. Lee, Y. S. Yang, and H. Y. Chu, Electrochem. Solid-State Lett. **8**, H21 (2005).
[11]M. D. Groner, S. M. George, R. S. McLean, and P. F. Carcia, Appl. Phys. Lett. **88**, 051907 (2006).
[12]E. Langereis, M. Creatore, S. B. S. Heil, M. C. M. van de Sanden, and W. M. M. Kessels, Appl. Phys. Lett. **89**, 081915 (2006).
[13]R. Matero, M. Ritala, M. Leskelä, T. Salo, J. Aromaa, and O. Forsén, J. Phys. IV **9**, 493 (1999).
[14]S. E. Potts, L. Schmalz, M. Fenker, B. Díaz, J. Światowska, V. Maurice, A. Seyeux, P. Marcus, G. Radnóczi, L. Tóth, and W. M. M. Kessels, J. Electrochem. Soc. **158**, C132 (2011).
[15]B. Díaz, E. Härkönen, J. Światowska, V. Maurice, A. Seyeux, P. Marcus, and M. Ritala, Corros. Sci. **53**, 2168 (2011).
[16]H. B. Profijt, S. E. Potts, M. C. M. van de Sanden, and W. M. M. Kessels, J. Vac. Sci. Technol. A **29**, 050801 (2011).
[17]S. E. Potts, W. Keuning, E. Langereis, G. Dingemans, M. C. M. van de Sanden, and W. M. M. Kessels, J. Electrochem. Soc. **157**, P66 (2010).
[18]D. Barreca, G. A. Battison, R. Gerbasi, and E. Tondello, J. Mater. Chem. **10**, 2127 (2000).
[19]W. Cho, K. Sung, K.-S. An, S. S. Lee, T.-M. Chung, and Y. Kim, J. Vac. Sci. Technol. A **21**, 1366 (2003).
[20]J. Koo, S. K. Kim, S. Joen, H. Jeon, Y. Kim, and Y. Won, J. Korean Phys. Soc. **48**, 131 (2006).
[21]B. Lux, C. Colombier, H. Altena, and K. Stjernberg, Thin Solid Films **138**, 49 (1986).
[22]K. H. Kim, C. H. Ho, T.-G. Suh, S. Prakash, and R. F. Bunshah, J. Mater. Eng. **13**, 199 (1991).
[23]E. Fredriksson and J.-O. Carlsson, Surf. Coat. Technol. **56**, 165 (1993).
[24]L. Tan, Y. Zan, J. Wang, Q. Wang, Y. Yu, S. Wang, Z. Liu, and L. Lin, J. Cryst. Growth **236**, 261 (2002).
[25]J. L. Dupuie and E. Gulari, Appl. Phys. Lett. **59**, 549 (1991).
[26]T. Stauden, G. Eichhorn, V. Cimalla, J. Pezoldt, and G. Ecke, Diamond Relat. Mater. **6**, 1210 (1996).
[27]K. Tsubouchi and K. Masu, Vacuum **46**, 1249 (1995).
[28]G. S. Higashi and C. G. Fleming, Appl. Phys. Lett. **55**, 1963 (1989).
[29]K. Sugioka, J.-F. Fan, K. Toyoda, H. Waki, and H. Takai, J. Mater. Res. **7**, 185 (1992).
[30]A. C. Dillon, A. W. Ott, J. D. Way, and S. M. George, Surf. Sci. **322**, 230 (1995).
[31]A. W. Ott, J. W. Klaus, J. M. Johnson, and S. M. George, Thin Solid Films **292**, 135 (1997).
[32]M. D. Groner, F. H. Fabreguette, J. W. Elam, and S. M. George, Thin Solid Films **413**, 186 (2002).
[33]M. D. Groner, F. H. Fabreguette, J. W. Elam, and S. M. George, Chem. Mater. **16**, 639 (2004).
[34]R. L. Puurunen, J. Appl. Phys. **97**, 121301 (2005).
[35]J.-F. Fan, K. Sugioka, and K. Toyoda, Jpn. J. Appl. Phys. **30**, L1139 (1991).
[36]L. Hiltunen, H. Kattelus, M. Leskelä, M. Mäkelä, L. Niinistö, E. Nykänen, P. Soininen, and M. Tiitta, Mater. Chem. Phys. **28**, 379 (1991).
[37]J. Kim, K. Chakrabarti, J. Lee, K.-Y. Oh, and C. Lee, Mater. Chem. Phys. **78**, 733 (2003).
[38]S. K. Kim and C. S. Hwang, J. Appl. Phys. **96**, 2323 (2004).
[39]S. K. Kim, S. W. Lee, C. S. Hwang, Y.-S. Min, J. Y. Won, and J. Jong, J. Electrochem. Soc. **153**, F69 (2006).
[40]J. Kwon, M. Dai, M. D. Halls, and Y. J. Chabal, Chem. Mater. **20**, 3248 (2008).
[41]D. M. Goldstein, J. A. McCormick, and S. M. George, J. Phys. Chem. C **112**, 19530 (2008).
[42]V. R. Rai and S. Agarwal, J. Phys. Chem. C **112**, 9552 (2008).
[43]A. Niskanen, K. Arstila, M. Ritala, and M. Leskelä, J. Electrochem. Soc. **152**, F90 (2005).
[44]S. B. S. Heil, P. Kudlacek, E. Langereis, R. Engeln, M. C. M. van de Sanden, and W. M. M. Kessels, Appl. Phys. Lett. **89**, 131505 (2006).
[45]J. L. van Hemmen, S. B. S. Heil, J. H. Klootwijk, F. Roozeboom, C. J. Hodson, M. C. M. van de Sanden, and W. M. M. Kessels, J. Electrochem. Soc. **154**, G165 (2007).
[46]E. Langereis, M. Bouman, J. Keijmel, S. B. S. Heil, M. C. M. van de Sanden, and W. M. M. Kessels, ECS Trans. **16**, 247 (2008).
[47]V. R. Rai and S. Agarwal, J. Phys. Chem. C **113**, 12962 (2009).
[48]C. Elschenbroich, *Organometallics*, 5th ed. (Wiley-VCH, Weinheim, 2005).
[49]P. H. Lewis and R. E. Rundle, J. Chem. Phys. **21**, 986 (1953).
[50]R. G. Vranka and E. L. Amma, J. Am. Chem. Soc. **93**, 3121 (1967).
[51]M. B. Smith, J. Organomet. Chem. **46**, 31 (1972).
[52]G. S. McGrady, J. F. C. Turner, R. M. Ibberson, and M. Prager, Organometallics **19**, 4398 (2000).
[53]A. W. Laubengayer and W. F. Gilliam, J. Am. Chem. Soc. **63**, 477 (1941).
[54]A. Almenningen, S. Halvorsen, and A. Haaland, Acta Chem. Scand. **25**, 1937 (1971).
[55]S. J. Yun, K.-H. Lee, J. Skarp, H.-R. Kim, and K.-S. Nam, J. Vac. Sci. Technol. A **15**, 2993 (1997).
[56]P. I. Räisänen, M. Ritala, and M. Leskelä, J. Mater. Chem. **12**, 1415 (2002).
[57]K.-E. Elers, T. Blomberg, M. Peussa, B. Aitchison, S. Haukka, and S. Marcus, Chem. Vap. Deposition **12**, 13 (2006).
[58]Y.-S. Min, Y. J. Cho, and C. S. Hwang, Chem. Mater. **17**, 626 (2005).
[59]R. Katamreddy, R. Inman, G. Jursich, A. Soulet, and C. Takoudis, J. Electrochem. Soc. **153**, C701 (2006).
[60]R. Katamreddy, R. Inman, G. Jursich, A. Soulet, A. Nicholls, and C. Takoudis, Thin Solid Films **515**, 6931 (2007).
[61]R. Katamreddy, R. Inman, G. Jursich, A. Soulet, and C. Takoudis, J. Mater. Res. **22**, 3455 (2007).
[62]J. H. Rogers, A. W. Apblett, W. M. Cleaver, A. N. Tyler, and A. R. Barron, J. Chem. Soc., Dalton Trans. 3179 (1992).
[63]D. A. Drew, A. Haaland, and J. Weidlein, Z. Anorg. Allg. Chem. **398**, 241 (1973).
[64]A. Haaland and O. Stokkeland, J. Organomet. Chem. **94**, 345 (1975).
[65]S. Y. Lee, B. Luo, Y. Sun, J. M. White, and Y. Kim, Appl. Surf. Sci. **222**, 234 (2004).
[66]J. Niinistö, K. Kukli, M. Kariniemi, M. Ritala, M. Leskelä, N. Blasco, A. Pinchart, C. Lachaud, N. Laaroussi, Z. Wang, and C. Dussarrat, J. Mater. Chem. **18**, 5243 (2008).
[67]E. Langereis, S. B. S. Heil, H. C. M. Knoops, W. Keuning, M. C. M. van de Sanden, and W. M. M. Kessels, J. Phys. D **42**, 073001 (2009).
[68]J. F. Moulder, W. F. Stickle, P. E. Sobol, and K. D. Bomben, *Handbook of X-ray Photoelectron Spectroscopy* (Physical Electronics, Chanhassen, MN, 1995).
[69]K.-S. An, W. Cho, K. Sung, S. S. Lee, and Y. Kim, Bull. Korean Chem. Soc. **24**, 1659 (2003).
[70]S. B. S. Heil, J. L. van Hemmen, M. C. M. van de Sanden, and W. M. M. Kessels, J. Appl. Phys. **103**, 103302 (2008).
[71]R. L. Puurunen, Appl. Surf. Sci. **245**, 6 (2005).
[72]O. J. Orient and S. K. Srivastava, J. Phys. B **20**, 3923 (1987).
[73]R. L. Puurunen, J. Appl. Phys. **95**, 4777 (2004).
[74]M. Ritala, M. Leskelä, L. Niinistö, and P. Haussalo, Chem. Mater. **5**, 1174 (1993).
[75]A. Yanguas-Gil and J. W. Elam, ECS Trans. **33**, 333 (2010).
[76]A. G. Davies and B. P. Roberts, J. Chem. Soc. B 1074 (1968).
[77]S. Yamashita, K. Watanuki, H. Ishii, Y. Shiba, M. Kitano, Y. Shirai, S. Sugawa, and T. Ohmi, J. Electrochem. Soc. **158**, H93 (2011).
[78]T. Gougousi, D. Barua, E. D. Young, and G. N. Parsons, Chem. Mater. **17**, 5093 (2005).
[79]V. R. Rai, V. Vandalon, and S. Agarwal, Langmuir **26**, 13732 (2010).
[80]R. Matero, A. Rahtu, M. Ritala, M. Leskelä, and T. Sajavaara, Thin Solid Films **368**, 1 (2000).
[81]L. Henn-Lecordier, M. Anderle, E. Robertson, and G. W. Rubloff, J. Vac. Sci. Technol. A **29**, 051509 (2011).
[82]C. Leguijt, P. Lölgen, J. A. Eikelboom, A. W. Weeber, F. M. Schuurmans, W. C. Sinke, P. F. A. Alkemade, P. M. Sarro, C. H. M. Marée, and L. A. Verhoef, Sol. Energy Mater. Sol. Cells **40**, 297 (1996).
[83]A. G. Aberle and R. Hezel, Prog. Photovoltaics **5**, 29 (1997).

[84]M. J. Kerr and A. Cuevas, Semicond. Sci. Technol. **17**, 166 (2002).
[85]J. D. Moschner, J. Henze, J. Schmidt, and R. Hezel, Prog. Photovoltaics **12**, 21 (2004).
[86]J. Zhao, A. Wang, and M. A. Green, Prog. Photovoltaics **7**, 471 (1999).
[87]H. Nagayoshi, M. Ikeda, M. Yamaguchi, T. Uematsu, T. Saitoh, and K. Kamisako, Jpn. J. Appl. Phys. **36**, 5688 (1997).
[88]B. Hoex, F. J. J. Peeters, M. Creatore, M. A. Blauw, W. M. M. Kessels, and M. C. M. van de Sanden, J. Vac. Sci. Technol. A **24**, 1823 (2006).
[89]T. C. Kho, S. C. Baker-Finch, and K. R. McIntosh, J. Appl. Phys. **109**, 053108 (2011).
[90]G. Dingemans, N. M. Terlinden, D. Pierreux, H. B. Profijt, M. C. M. van de Sanden, and W. M. M. Kessels, Electrochem. Solid-State Lett. **14**, H1 (2011).
[91]B. Hoex, J. J. H. Gielis, M. C. M. van de Sanden, and W. M. M. Kessels, J. Appl. Phys. **104**, 113703 (2008).
[92]P. Saint-Cast, D. Kania, M. Hofmann, J. Benick, J. Rentsch, and R. Preu, Appl. Phys. Lett. **95**, 151502 (2009).
[93]T.-T. Li and A. Cuevas, Phys. Status Solidi RRL **3**, 160 (2009).
[94]D. W. Squire, C. S. Dulcey, and M. C. Lin, J. Vac. Sci. Technol. B **3**, 1513 (1985).